The phase separation behaviour and the viscoelastic properties of particles with non-adsorbing polymers: Part I — Experimental study

J.W. Goodwin, R.W. Hughes *, H.M. Kwaambwa, P.A. Reynolds

University of Bristol, Bristol Colloid Centre, School of Chemistry, Cantock's Close, Bristol BS8 1TS, UK

Abstract

A series of well characterised *cis*-polyisoprene polymers have been added to dispersions of PHS coated PMMA particles in dodecane. At a molecular weight of 8000 g mol^{-1} and above, these systems showed phase separation at low particle volume fractions and above a critical polymer concentration. The rate of separation has been shown to be influenced by the viscosity of the polymer. At high polymer and particle volume fractions long lived metastable phases occurred. Above a critical concentration these were viscoelastic indicating an appreciable change in diffusion dynamics with two relaxation processes present. A significant Bingham yield stress was also observed. The Asakura Oosawa potential was not able to describe the observed rheological properties. At a molecular weight of 1000 g mol^{-1} no phase separation was observed. At high particle concentrations the yield stress was found to reduce with the addition of polymer. This was due to the polymer acting as a 'solvent' and penetrating the stabilising layer on the particles.

Keywords: Non-absorbing polymers; Phase separation; Viscoelastic properties; Depletion; Rheology

1. Introduction

This is the first in a series of papers reporting the rheological properties of a depletion system. The addition of a non-adsorbing polymer to a dispersion of particles can induce phase separation. This occurs at a concentration c^* where the polymers form a connected structure throughout the system. This might be expected to occur when the attractive energy between the particles is of the order of a few kT. For particles denser than the medium the phase separation is normally observed by the sedimentation of the particles. As the concentration of polymer is increased the apparent phase separation is no longer so rapid. Eventually if a density difference exists between the medium and the particles and in the absence of any other significant pair interaction forces sedimentation will be observed. Explanations for this behaviour have been linked with the notion of a depletion layer. This is where the concentration of polymer close to the surface of a particle will be depleted in the absence of a surface excess

* Corresponding author. Tel.: +44-117-928-9936.
E-mail address: r.w.huges@bristol.ac.uk (R.W. Hughes)

concentration. This results in a layer around the particle with a thickness of the order of twice the radius of gyration of the polymer which is depleted of polymer. When two particles undergoing Brownian movement approach closer than twice the radius of gyration, the polymer coil will be excluded from this depletion layer. There will be an excess osmotic pressure acting on the particles from the polymer. This arises since there is a higher concentration of polymer in the bulk than in the layer overlap region between the particles. These particles tend to aggregate and thus sedimentation occurs at a faster rate. The attractive depletion potential that results has been modelled with varying degrees of complexity. For dilute polymers the simplest approach is to replace the polymer coils by an equivalent hard sphere and determine from the particle geometry the force that arises when the depletion layers overlap. Asakura and Oosawa (AO) [1,2] presented a simple expression for this which was later generalised by Vrij [3]. This expression is:

$$V(r) = -\Pi\left(\frac{4\pi}{3}\right)\left((a+R_g)^3 - \frac{3r}{4}(a+R_g)^2 + \frac{r^3}{16}\right) \quad 2R_g \geq r \geq 2a \tag{1}$$

where Π is the osmotic pressure of the polymer, R_g the radius of gyration, a the particle radius and r the centre to centre separation. It describes the variation in the pair interaction energy between two colloidal particles.

There are two approaches for improving the quality of the description of the pair potential. The first improvement was by de Gennes et al. [4] allowing for the internal degrees of freedom of the polymer coil. This also allows for the reduction in the polymer dimensions in the semi-dilute regime. This gives results consistent with the AO approach. The second improvement is to allow for concentration effects. These can manifest themselves in several ways. Firstly above c^* the coil will begin to collapse in a theta solvent to avoid interpenetration of the coils. Secondly as the concentration is increased the coils interact and show a variation in their spatial distribution. The equivalent system of hard spheres would develop a pair distribution function with fluctuations in the local number density. Of course this distribution function will be changed by the presence of the particle surface. This can be treated as a hard wall. Since a variation in the pair distribution function will lead to local variations in the osmotic pressure, the interparticle force curve between the particles becomes more complex. In principle it is feasible for repulsion to occur between the particles. If this model is taken to the dilute limit, it is consistent with that developed by Asakura and Oosawa.

Rheological measurements which are performed at low stress or strain are very sensitive to the form of the pair interaction potential. These techniques represent a good method of investigating, albeit indirectly, the pair potential between the particles in a system with non-adsorbing polymer. These studies present an interesting picture of the behaviour of the systems as the concentration of polymer is increased. They can be performed on systems with transient stability with respect to the depletion induced phase separation and so they can measure the properties of metastable systems. For a dispersion of hard sphere colloidal particles the onset of shear thinning is observed at a volume fraction of about $\phi = 0.40$. However when non-adsorbing polymer is added to these systems shear thinning can be observed to occur earlier depending upon the concentration of polymer that has been added. The flow curve allows the extrapolation of the data to an apparent Bingham yield stress. This has been observed by Tadros, Luckham and Liang [5–7]. They modelled the system using an approach first developed by Michaels and Bolger [8] which indicates a dependence on the square of the particle volume fraction and a direct proportionality to the depth of the attractive interaction between the particles. They were not able to reproduce this correlation. Indeed their data indicated a critical concentration of polymer was required before a significant yield stress was observed. The same phenomena has been observed in aggregation by Sperry et al. and others [9,10]. This presents a conundrum, as the AO potential and its variants are continuous in concentration, the yield stress may also be expected to be a continuous function of concentration.

In this paper the rheological influences on the depletion phenomena are considered. The next paper in the series considers an alternative approach for evaluating the depletion potential which serves to illustrate some of the possible failings of the AO approach.

2. Experiments and results

2.1. Characterisation of the dispersions

Five PMMA lattices sterically stabilised with chemically grafted PHS chains and dispersed in dodecane were prepared using the method described by Antl et al. [11]. The PHS chains are terminally grafted at multiple points along the backbone of an insoluble anchor polymer PMMA. Three 'comb-like' PHS stabilisers (code names I, II and ICI) of varying degrees of polymerisation were used. Stabilisers I and II were prepared in our laboratory whereas stabiliser ICI was supplied by Dr Neil Perrins, ICI Paints Division, Slough. The particle core radius, a, was determined by transmission electron microscopy (TEM). The particles core volume fraction was derived by drying in a vacuum oven a sample of known weight and knowledge of the densities of PMMA core particles ($\rho = 1.18$ g cm^{-3}) and dodecane ($\rho = 0.749$ g cm^{-3}). The adsorbed layer thickness, δ, was determined by using a method based on the Krieger–Dougherty viscosity–concentration relationship [12]. The particles were dispersed in dodecane at a range of concentrations. The approach adopted was to assume the high shear viscosity relative to the solvent was given by the Krieger–Dougherty equation.

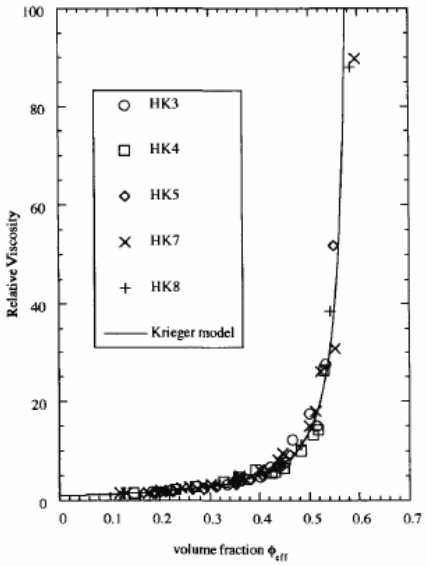

Fig. 1. The relative high shear rate viscosity against effective volume fraction.

$$\eta_r = \left(1 - \frac{\phi_{\text{eff}}}{\phi_{\text{m}}^{\infty}}\right)^{-[\eta]\phi_{\text{m}}^{\infty}} \tag{2}$$

The intrinsic viscosity $[\eta] = 2.5$ and ϕ_{m}^{∞} is the packing fraction of the particles in the high shear limit. If it is assumed the particles move in layered flow in this limit the maximum packing fraction is $\phi_{\text{m}}^{\infty} = 0.605$ [13]. The effective volume fraction ϕ_{eff} is the volume fraction of the core of the particles of PMMA/PHS as determined by dry weight, ϕ, plus the increase in volume fraction due to the solvation of the PHS shell. This is given by:

$$\phi_{\text{eff}} = \phi\left(1 + \frac{\delta}{a}\right)^3 \tag{3}$$

Thus by fitting the viscosity concentration curve to Eq. (2) the effective volume fraction is determined. This plot is shown in Fig. 1. Since the volume fraction of the core PMMA is known the adsorbed layer thickness can be obtained by rearrangement of Eq. (3). The particle characterisation data are given in Table 1.

2.2. Characterisation of the polymers

The added free polymer was *cis*-poly(isoprene) (PIP) and was obtained from Polymer Laboratories, together with molecular weight characterisation data. PIP was chosen for three main reasons.

1. It is soluble in dodecane (solubility parameters are very similar [14]).

Table 1
Particle characterisation data based on high concentration viscometry experiments

Latex code	a (nm)	COV (%)[a]	Stabiliser code	δ (nm)	PHS chain (M_w)	a/δ
HK3	405	4.7	I	14	3100	29
HK4	267	5.8	I	14	3100	19
HK5	180	8.5	II	3.5	680	51
HK7	116	12.2	ICI	4	1800	29
HK8	156	9.2	ICI	6	1800	26

[a] COV is the coefficient of variation = 100 × SD deviation/radius).

2. There is little or no adsorption of the polymer to the particles probably due to its low functionality.
3. The polydispersity (ratio of weight-average to number average molecular weights, $M_w/M_n < 1.10$) was low over the molecular weight range of interest.

The density of polymer was 0.91 g cm^{-3}. The molecular weights were chosen such that there were situations where the polymer radius of gyration R_g is roughly equal to δ. R_g values were derived from measured intrinsic viscosities. For a given polymer molecular weight, the relative solution viscosity of PIP in dodecane at 298 K was measured using capillary viscometry. This was performed at several polymer concentrations. These data were extrapolated linearly by Huggins and Kraemer plots [14,15] to find the intrinsic viscosity at infinite dilution $[\eta]$. This was performed for each molecular weight and the intrinsic viscosity was plotted using the Mark–Houwink equation allowing for the low molecular weight coil rigidity which gave:

$$[\eta] = 1.0 + 0.0158 M_v^{0.72} \quad g^{-1}\ cm^3 \tag{4}$$

for $1180 \leq M_w \leq 115\,000$ where M_v is the viscosity average molecular weight. The intercept allows for the rigidity of the chain at low molecular weights. The power index 0.72 indicates that dodecane is a good solvent for PIP and the latter exists in solution as open flexible random coil. The Stockmayer–Fixman equation can also be applied to the data. This is given by:

$$[\eta] = K_o M^{0.5} + 0.51 \Phi B M \quad g^{-1}\ cm^3 \tag{5}$$

with the constant $\Phi = 2.5 \times 10^{23}$ mol^{-1}. This equation is linearised in Fig. 2[16]. This gave an intercept of $K_o = 0.101$ cm^3 mol$^{0.5}$ g$^{-1.5}$ and a value of $B = 2.60 \times 10^{32}$ cm^3 mol^2 g^{-2}.

Table 2 shows the molecular weight data supplied with the respective extrapolated intrinsic viscosities and calculated polymer dimensions. The hydrodynamic radius R_h is determined assuming the polymer coils are hard spheres so that when the polymer coil concentration is represented in terms of a volume fraction the extrapolated intrinsic viscosity is the Einstein value of 2.5. This gives an equivalent hydrodynamic radius of,

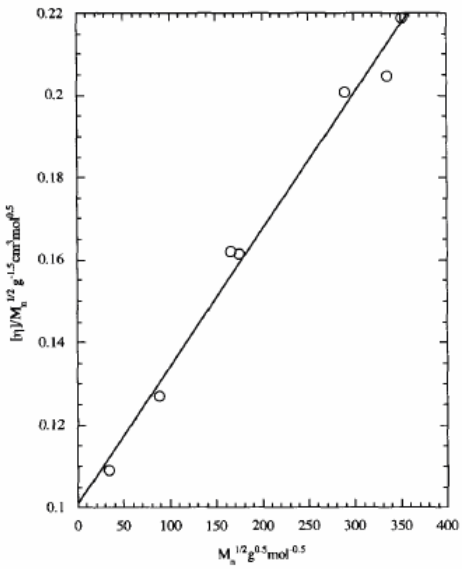

Fig. 2. The Stockmayer–Fixman plot for PIP.

Table 2
Characteristic properties of PIP in dodecane

Polymer code	M_w (g mol^{-1})	M_v (g mol^{-1})	M_w/M_n	$[\eta]$ (cm^3 g^{-1})	R_h (nm)	R_{go} (nm)	R_g (nm)
P1K	1180	1203	1.08	3.61	0.9	1.0	1.1
P8K	8000	8308	1.03	11.19	2.4	2.9	3.2
P28K	28300	29 103	1.03	26.86	4.9	5.9	7.0
P31K	31 500	31 257	1.03	28.23	5.3	6.4	7.7
P86K	86 000	87 862	1.02	58.30	9.2	11.0	14.5
P115K	115 000	110 000	1.02	68.37	10.7	12.8	17.4
P130K	130 000	–	1.05	76.98[a]	11.5	13.7	18.9

[a] Extrapolated data using Eq. (4).

Table 3
A polynomial fit to the viscosity of PIP solutions in dodecane

Polymer code	m_0 (mPa s)	m_1 (mPa s g^{-1} cm^3)	m_2 (mPa s g^{-2} cm^6)	m_3 (mPa s g^{-3} cm^9)	Maximum concentration (g cm^{-3})[a]
P1K	1.56	7.28	0.319	2.86	1.20
P8K	1.64	15.3	76.7	−9.79	0.60
P28K	1.52	31.4	363	422	0.22
P86K	1.60	5.72	2704	8592	0.15
P115K	1.50	2.90	3764	26348	0.15

[a] This refers to the maximum concentration used to determine the viscosity. It is the mass of polymer added to a unit volume of solvent.

$$R_h = \left(\frac{1}{2.5N_a}\frac{3[\eta]M_w}{4\pi 10^6}\right)^{1/3} \quad (6)$$

This gives the equivalent hard sphere diameter for the chain. Eq. (5) enables the calculation of the radius of gyration of the chain in theta conditions denoted by R_{go} and in dodecane R_g. These data are also shown in Table 2.

At higher concentrations the viscosity was measured using a Bohlin VOR and a Bohlin CS rheometer. These showed very slight shear thinning from the polymer. At the low shear rate the viscosity of the polymer solution can be fitted by a polynomial of the form:

$$\eta_p = m_0 + m_1 c + m_2 c^2 + m_3 c^3 \quad (7)$$

The coefficients m_i are given in Table 3 and c is the concentration of polymer as the mass of polymer is added to 1 cm^3 of dodecane. This function enables the viscosity to be interpolated for any given polymer concentration up the maximum value which was measured which is also given in Table 3. The correlation coefficient of the fit was very close to unity in all instances. It should be noted that any differences in the dilute limiting values of the viscosity as indicated by m_0 from that predicted by Eq. (4) result from the uncertainty in fitting the data using a polynomial. It should be noted that in the dilute limit Eq. (4) represents the most accurate description of the polymer viscosity.

2.3. Phase separation

The phase separation behaviour of the various PMMA dispersions was studied in the presence of the added polymer. A stock dispersion of latex of known volume fraction and high PIP concentration was prepared. The samples were then prepared in similar screw-top, glass vials. The required amounts of stock dispersion, latex dispersion and polymer were added gravimetrically (weighing the vial after each addition). The samples were allowed to stand at room temperature. The data for the ratio of sediment height (H_S) to

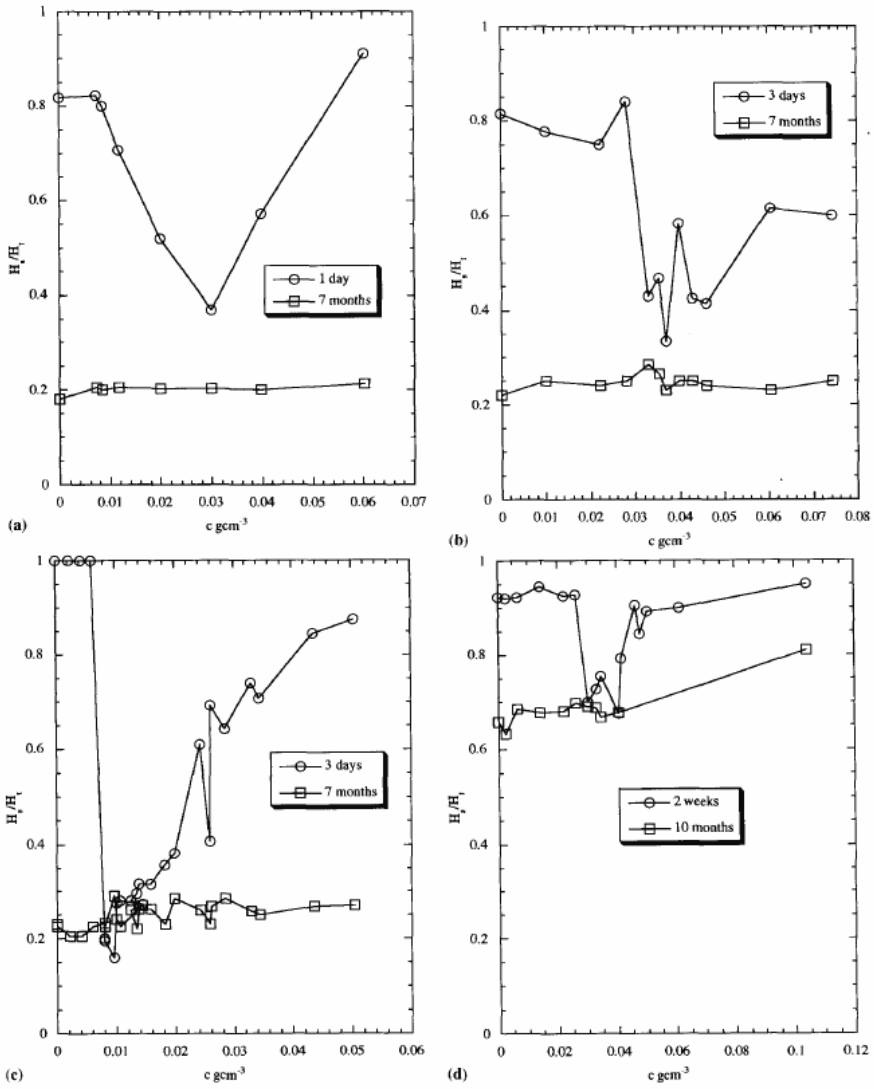

Fig. 3. (a) Phase separation results for HK3 at a volume fraction of $\phi = 0.116$ with the added concentration of the polymer P86K. (b) Phase separation results for HK4 at a volume fraction of $\phi = 0.123$ with the added concentration of the polymer P28K. (c) Phase separation results for HK5 at a volume fraction of $\phi = 0.104$ with the added concentration of the polymer P86K. (d) Phase separation results for HK5 at a volume fraction of $\phi = 0.344$ with the added concentration of the polymer P28K.

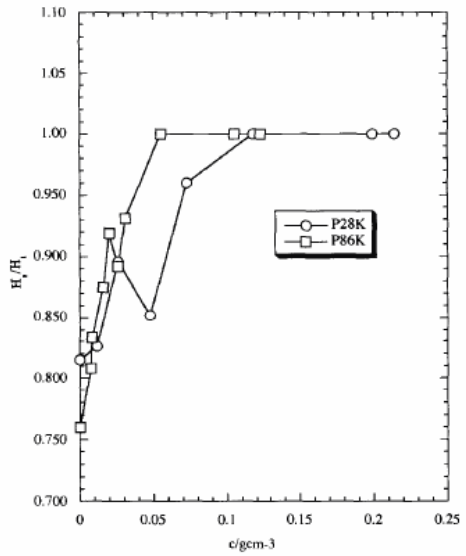

Fig. 4. Phase separation results for HK4 at a volume fraction of $\phi = 0.425$ with the added concentration of the polymer P28K and P86K.

nism with a combination of sedimentation and aggregation occurring. For smaller particle sizes that exhibited two phases for instance HK7 to HK4 with added polymer P8K a crude estimate of c^+ was found to be in the range 0.06–0.09 g cm^{-3}. The form of the phase separation curve shows a sharp breakpoint at a critical concentration giving marked phase separation. At higher concentrations there is an increase in the height of the phase boundary followed by a reduction. With time the shape of the curve is maintained but the sediment boundary height has reduced across the whole concentration range. Presumably this is due to sedimentation.

2.3.3. The results with the addition of P1K

There was no phase separation when P1K was used as the added polymer for any latex system. The results discussed above seem to agree with the observations of Reynolds and Reid [18] for low molecular weight polymer. The results here support the notion that phase separation phenomenon fails if the molecular weight of the added polymer is relatively low.

2.4. Rheological characterisation

The rheological measurements were made using a Bohlin VOR rheometer and a Rank Brothers Pulse Shearometer. The Bohlin rheometer was used to measure the shear stress as a function of the applied shear rate. The linear viscoelastic response was determined by dynamic oscillatory measurements. The Pulse Shearometer was used to measure the wave rigidity modulus and the high frequency limit to the shear modulus, $G(\infty)$. Latex dispersions were made such that the particle volume fraction was in the range 0.35–0.53. In this region, the particle concentrations are still large enough for the interactions to be significant with no compression of the adsorbed layer but the rheology of the system is relatively insensitive to

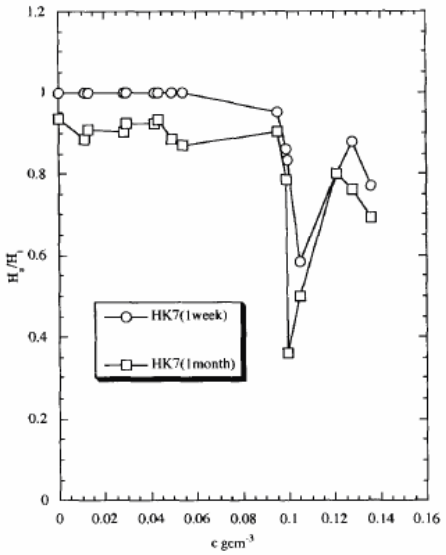

Fig. 5. Phase separation results for HK7 at a volume fraction of $\phi = 0.237$ with the added concentration of the polymer P8K.

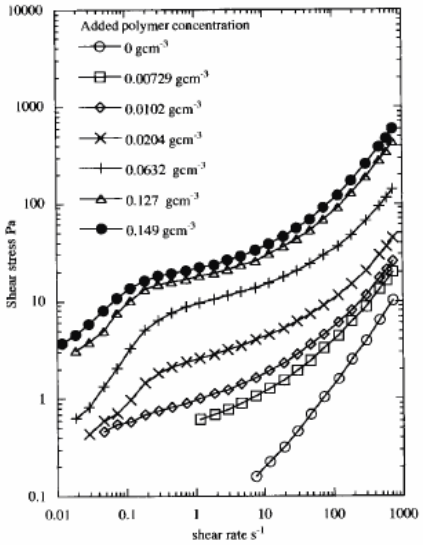

Fig. 6. Shear stress versus shear rate for HK4 (log – log) at a volume fraction of $\phi = 0.377$ with the added concentration of the polymer P115K.

small solvent losses. The polymer concentration in the continuous phase was varied over a wide range to cover, if possible, the dilute, semi-dilute and concentrated regimes [19,20]. The volume fraction of the particles was chosen such that no phase separation of the systems were seen during the measurements. All rheological measurements were carried out at 25.0 ± 0.1°C except for the wave rigidity modulus which was measured at 20.0 ± 1°C.

2.5. Viscometric characterisation

Three designs of the instrument geometry were used in this study: a cone and plate; a double concentric cylinder and; a bob and cup (single concentric cylinders). The viscosity of the samples was determined by applying a known strain rate to the sample and the resulting stress was measured. Each viscometric run was commenced at the lowest shear rate and increased successively to higher shear rates to obtain a flow curve.

2.5.1. High molecular weight characterisation

A typical example of a shear stress–shear rate curve for PMMA dispersions with added polymer ($M_w \geq 8000$ g mol^{-1}) is shown in Fig. 6. The log of the shear stress is plotted against the log of the shear rate. This shows the material is psuedoplastic and developing a measurable low shear viscosity at low shear rates. A plot of shear stress versus shear rate in Fig. 7 shows there is a linear relationship between shear stress and shear rate once a shear rate of about 50 s^{-1} is exceeded. This is true for all the high molecular weight high concentration samples investigated. The data above 50 s^{-1} could be fitted to the Bingham equation.

$$\sigma = \sigma_B + \eta_{pl}\dot{\gamma} \quad (8)$$

where σ_B is the Bingham yield stress, η_{pl} is the high shear limiting viscosity and $\dot{\gamma}$ is the shear rate. In the high shear limit the relative viscosity approaches that of quasi-hard sphere systems.

A typical example of the relationship between σ_B and the added polymer concentration for the

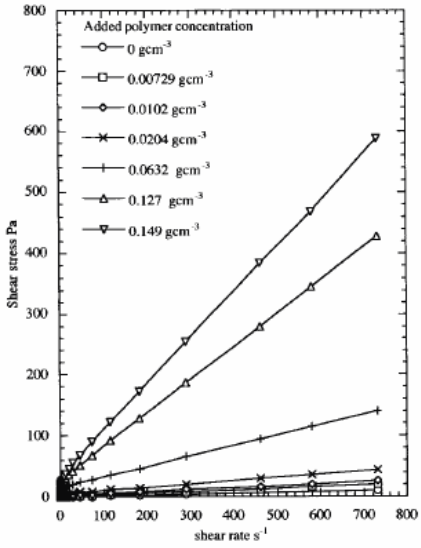

Fig. 7. Shear stress versus shear rate for HK4 at a volume fraction of $\phi = 0.377$ with the added concentration of the polymer P115K.

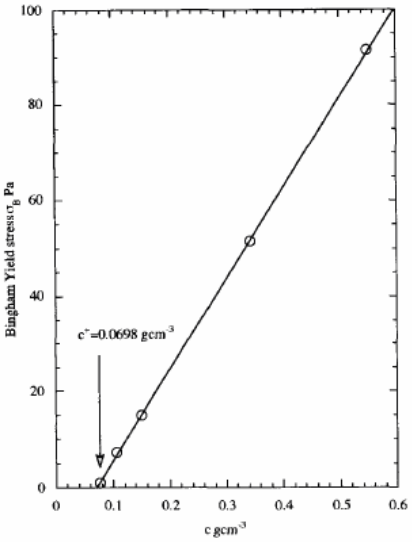

Fig. 8. A plot of Bingham yield stress as a function of added polymer (P8K) to HK7 at a volume fraction $\phi = 0.416$.

systems with polymers of molecular weights greater than that of P1K is shown in Fig. 8. There is a rapid and linear increase in σ_B with an increase in polymer concentration when the latter exceeds a critical value c^+. The critical concentration c^+ was taken as the concentration at which the polymer begins to induce depletion flocculation or instability as in the case of phase separation experiments.

The effect of molecular weight of added polymer to c^+ value is shown in Fig. 9 for latex HK4 with added polymers P28K and P86K. The higher the molecular weight of the added polymer, the lower the value of c^+ for a given latex dispersion. At any given polymer concentration above c^+, σ_B is always greater for the system with higher molecular weight polymer. The Bingham yield stress σ_B increases with increase in particle volume fraction ϕ at the same added polymer concentration. For instance, the Bingham yield stress data is shown in Fig. 10 for latex HK4 with added polymer P86K. The results shown in Fig. 11 for lattices HK3 and HK4 show the Bingham yield stress with added polymer P28K. This data shows that the value of c^+ found from the Bingham yield stress is not constant for a given molecular weight but it is a function of latex particle size.

Table 5 summarises the values of c^+ determined using σ_B data for different latex and polymer combinations. It is important to note that the critical concentrations derived this way for different latex/polymer combinations are similar in terms of behaviour and magnitude as a function of polymer molecular weight to those observed to induce phase separation although the latter was at low particle volume fractions ($\phi < 0.35$).

2.5.2. Low molecular weight characterisation (P1K)

The stress shear rate curve is shown in Fig. 12. This data is markedly different from that for the high molecular weight systems. In this system as the polymer concentration added is increased the

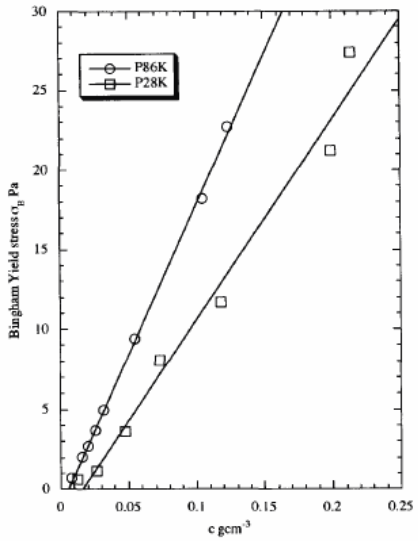

Fig. 9. A plot of Bingham yield stress as a function of added polymer (P28K and P86K) to HK4 at a volume fraction $\phi = 0.425$.

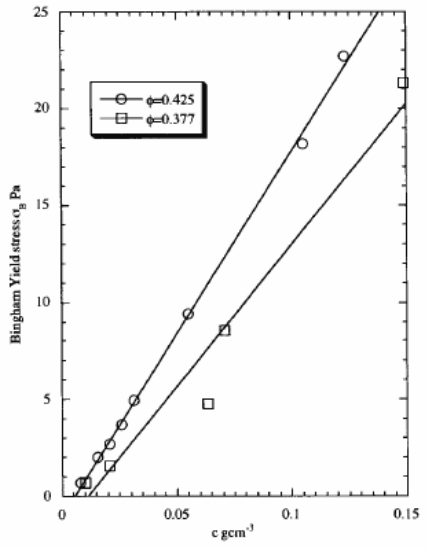

Fig. 10. The effect of volume fraction on the Bingham yield stress of latex HK4 and added P86K polymer.

flow curve and the Bingham yield stress *reduces* in value.

2.6. Dynamic oscillatory measurements

2.6.1. Strain sweeps

In order to establish the extent of the linear regime an oscillating strain of increasing magnitude and fixed frequency ω was applied to the sample. Fig. 13 shows a typical strain sweep at $\omega = 2\pi$ rad s^{-1} for PMMA dispersions with added PIP for high molecular weights. The curves display viscoelastic behaviour which was observed when the added polymer concentration was well above c^* and close to and above c^{**}. The concentration c^{**} represents the boundary between semi dilute and concentrated behaviour. There are several significant features to the plots. At low strains in the region where the storage modulus tends to a plateau value, the storage modulus G' and the complex modulus G^* equate. The linear region is small compared with charged stabilised systems [21] and Aerschot and Mewis [22] have suggested that this is characteristic of flocculated systems although the curves show a shape characteristic of many particulate systems [21]. The loss modulus

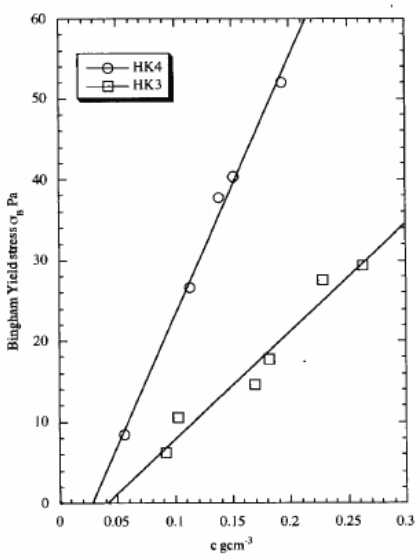

Fig. 11. The effect of particle size on the Bingham yield stress of latex HK4 and HK3 with added P28K polymer at a volume fraction $\phi = 0.435$.

Table 5
Critical polymer concentrations extrapolated from Bingham yield stress–polymer concentration data for PMMA dispersions with added polymer

Latex	Polymer	ϕ	ϕ_{eff}	c^+ (g cm^{-3})
HK4	P115K	0.448	0.522	0.00804
HK4	P115K[a]	0.377	0.439	0.0102
HK4	P86K	0.425	0.495	0.00533
HK4	P86K	0.377	0.439	0.0111
HK5	P86K	0.429	0.454	0.0107
HK3	P28K	0.435	0.481	0.0402
HK4	P28K	0.435	0.507	0.0277
HK4	P28K	0.425	0.495	0.0153
HK5	P28K	0.439	0.465	0.0303
HK7	P8K[a]	0.416	0.460	0.0698

[a] Note for P8K $c^* = 0.0757$ g cm^{-3}, and for P115K $c^* = 0.00633$ g cm^{-3}.

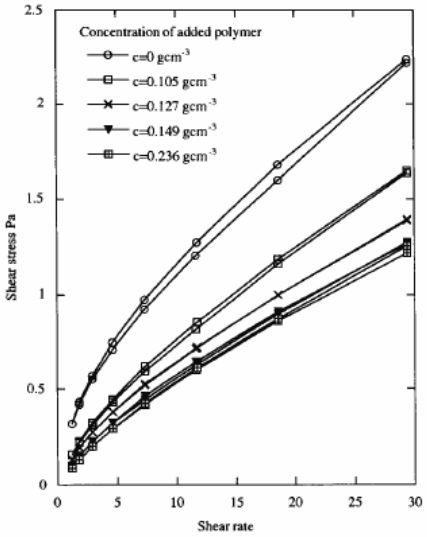

Fig. 12. Shear stress versus shear rate for HK8 at an initial volume fraction of $\phi_{eff} = 0.531$ with the added concentration of the polymer P1K.

displays a bell shaped curve which crosses over the sigmoidal shaped storage modulus. The cross over is termed the melting strain where the viscous and elastic processes balance. The onset of non-linearity occurs at a critical value of this strain γ_{crit} where the storage modulus markedly reduces. Establishing the linear region is important for subsequent oscillatory measurements since this allows simpler interpretation of the observed material response. The linear region was frequency independent for $\omega < 4\pi$ rad s^{-1} both in range and magnitude of the storage modulus in the plateau region. Once this frequency was exceeded the collected data was less reproducible. The most probable reason for this was a combination of instrumental and material constraints. The sample volumes available in this study were too small to allow the optimum instrument configuration to be adopted. An increase in polymer concentration resulted in an increase in the magnitudes of both G' and G''. The systems were dominantly elastic.

2.6.2. Oscillation measurements

The frequency dependence of the storage and loss moduli was measured in the linear region. It was possible to obtain data for oscillation tests for samples with an added polymer concentration $c > c^*$. At concentrations less than c^* the viscoelastic properties were below the range of instrument sensitivity. The change was marked and is indicative of a step change in material behaviour close to this concentration however it was not possible to verify this change unambiguously experimentally. Typical oscillation test curves are shown in Fig. 14. This data illustrates the general form of the curves. There is evidence for two relaxation processes at low and high frequencies. Unfortunately both these processes lie outside the instrumental range for the majority of the data. The loss modulus increases at both low and high frequencies and there is a plateau region in the storage modulus between these zones. Several researchers have observed similar trends [6,23–25]

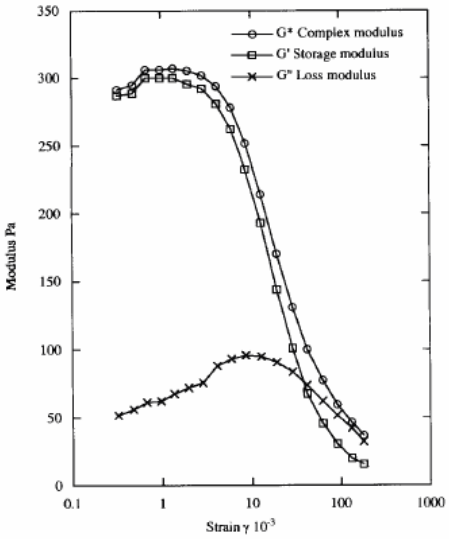

Fig. 13. A typical strain sweep at $\omega = 2\pi$ rad s^{-1} for HK3 with P86K, $\phi = 0.387$ and an added polymer concentration of $c = 0.149$ g cm^{-3}.

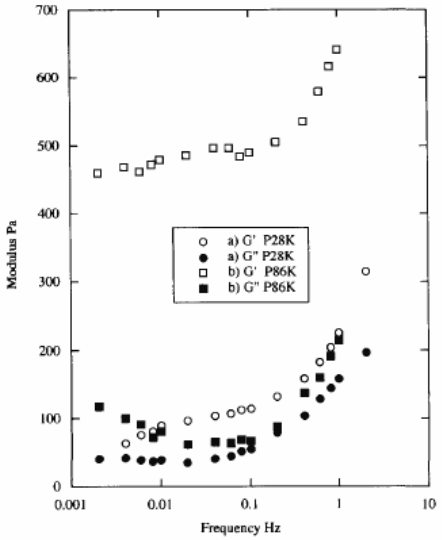

Fig. 14. Storage modulus (G') and loss modulus (G'') for dispersion HK5 with added PIP. The two systems are (a) P28K, $\phi = 0.475$, $c = 0.117$ g cm^{-3} and (b) P86K, $\phi = 0.479$, $c = 0.0628$ g cm^{-3}.

for latex dispersions depending on particle concentration. This region can disappear and be replaced by an ever increasing modulus depending upon the relative values of volume fraction, particle size and polymer concentration.

The effect of increasing polymer concentration between 0.002 and 2 Hz is shown in Fig. 15. The data is plotted as the loss modulus versus the storage modulus. The data shows the two processes seen above, which is typified by an increasing loss modulus gradually plateauing followed by a further increase in the loss modulus. An increase in polymer concentration at constant volume fraction results in increase in G' and G''. Both G' and G'' increase with decreasing particle size and increase in volume fraction at the same added polymer concentration.

In Fig. 16, the effect of particle size on both G' and G'' is shown whereas in Fig. 17 the effect of ϕ on G' is shown which indicates that as the volume fraction is increased the elasticity increased.

2.7. Pulse shearometer

The high frequency shear modulus for the dispersion was established by using a Rank Bros. Shearometer. In this technique a dispersion was placed between two parallel plates. A small shear strain impulse of about 10^{-4} was applied to the lower plate and the propagation time of this deformation through the sample was determined at a fixed separation. This process was repeated at a range of separations. This allowed a plot of distance between the plates versus propagation time to be constructed. The slope of this curve gives the velocity of the travelling wave. The product of the square of the velocity with the density of the sample gives the wave rigidity modulus. Provided the sample is domi-

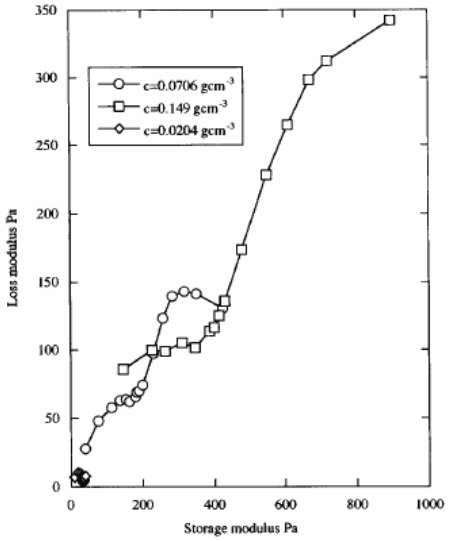

Fig. 15. The loss modulus versus the storage modulus for dispersion HK4 with added P86K and $\phi = 0.377$.

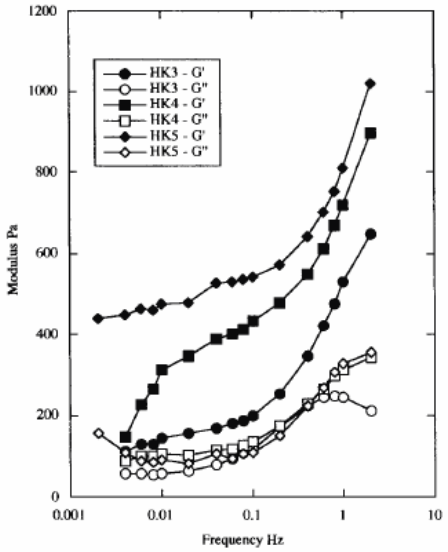

Fig. 16. The effect of particle size on the storage and loss moduli with an added polymer concentration of $c = 0.149$ g cm^{-3} and HK5 $\phi = 0.385$, $\phi_{eff} = 0.408$, HK4 $\phi = 0.377$, $\phi_{eff} = 0.439$, HK3 $\phi = 0.387$, $\phi_{eff} = 0.429$.

nantly elastic so that $G''$is insignificant the rigidity modulus can be equated with the high frequency limit of the network $G(\infty)$. This was true for all the data recorded here. The operating frequency for this instrument is about 1200 rad s^{-1}. This frequency is two orders of magnitude larger than the maximum value readily measured using a frequency sweep on the Bohlin VOR given the sample constraints. The form of the curves seen for the samples as a function of frequency suggests that the value recorded is at a frequency greater than the characteristic frequency for the fastest process. The measurements were made as both a function of volume fraction and polymer concentration.

The variation in rigidity modulus with volume fraction is shown in Fig. 18. Below about $\phi = 0.3$ rigidity moduli were not available as there was a rapid increase in the fluidity of the sample. At the same volume fraction of particles with no added polymer there was no significant elasticity. It arises due to the addition of polymer. Each set of data has been fitted to a power law relationship. This gives the expression:

$$G(\infty) \cong \tilde{G} = A\phi_{eff}^{m} \quad (9)$$

where $\tilde{G}$ is the wave rigidity modulus, which to a good approximation can be equated to the high frequency limit of the shear modulus. The term A is a constant representative of the strength of the structure. The constants for this system are given in Table 6. From this the value of the exponent lies in the range of 2.2–2.9. This is an agreement with the values for weak flocculation found by Russel and Sonntag [26] and Vold [27,28] from simulation data. Figs. 19 and 20 show the effect of polymer concentration on elasticity. These data show a feature also seen with the Bingham yield data which is that there is a critical concentration at which the moduli rapidly increases.

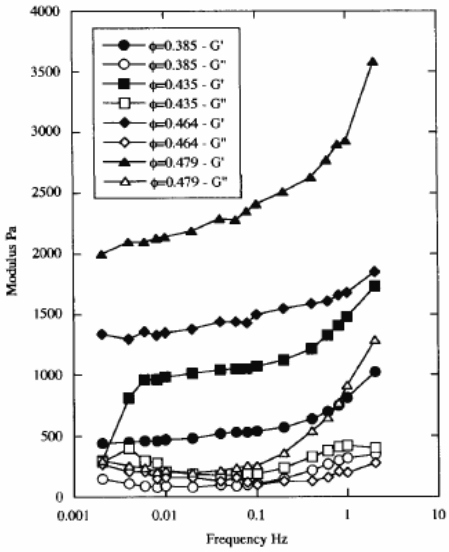

Fig. 17. The effect of volume fraction on the storage and loss modulus of HK5 with P86K and a concentration of added polymer of $c = 0.0149$ g cm^{-3} at a range of volume fractions.

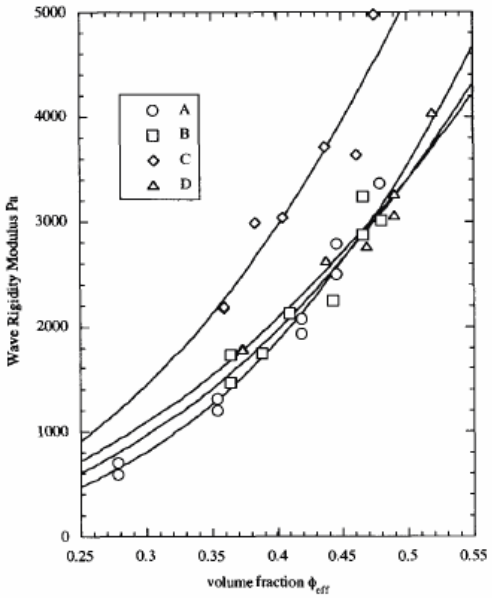

Fig. 18. A plot of the wave rigidity modulus as a function of volume fraction of HK5 for four systems: (A) P130K, $c = 0.0560$ g cm^{-3}; (B) P86K, $c = 0.0560$ g cm^{-3}; (C) P86K, $c = 0.0764$ g cm^{-3}; (D) P28K, $c = 0.105$ g cm^{-3}. The solid lines are power law fits given in Table 6.

Table 6
A power law fit to the shearometry data

Polymer	M_w (g mol^{-1})	c (g cm^{-3})	A (kPa)	m
P28K	28 300	0.105	28.9	2.49
P86K	86 000	0.0560	16.0	2.23
P86K	86 000	0.0764	19.0	2.48
P130K	130 000	0.0560	26.4	2.90

3. Discussion

3.1. Phase separation behaviour

The low molecular weight data on P1K shows no phase separation. In fact there were no responses observed consistent with depletion phenomena. This point will be examined more closely when the Bingham yield point data are considered. The ratio a_{eff}/R_g or its inverse is often used to demarcate the zones of phase behaviour observed with a latex along with the concentration of the species present. For P1K this ratio does not appear to be indicative of the change. The characterisation data for PIP emphasises that there is no apparent singularity or change in the material behaviour at low molecular weights, the Stockmayer–Fixman plot showing a good linearisation of the data. The values found are consistent with high molecular weight data in the literature [29]. A tentative suggestion is that as R_g approaches the adsorbed layer thickness δ that the polymer is able to penetrate the layer to an extent. Thus a well defined depletion zone no longer occurs. Clearly the degree of penetration should depend on the graft density in the layer, the polymer conformation and the relative solvency. Perhaps a reasonable guide for a rigid graft is that depletion will fail when $\delta/R_g \geq 1$.

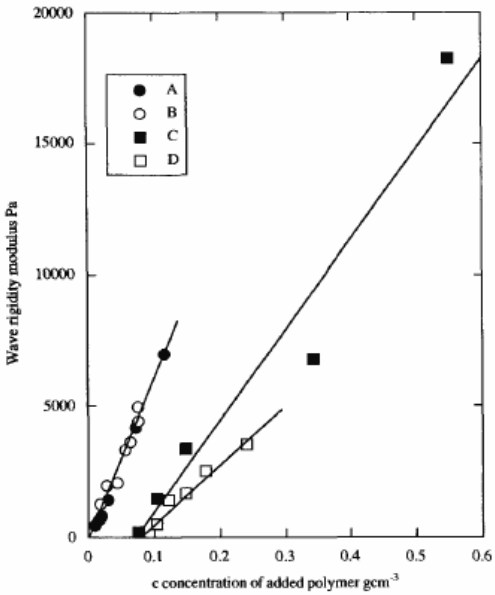

Fig. 19. A plot of the wave rigidity modulus as a function of polymer concentration for four systems: (A) HK5 P86K $\phi = 0.429$; (B) HK7 P86K $\phi = 0.416$; (C) HK7 P8K $\phi = 0.416$; (D) HK8 P8K, $\phi = 0.392$.

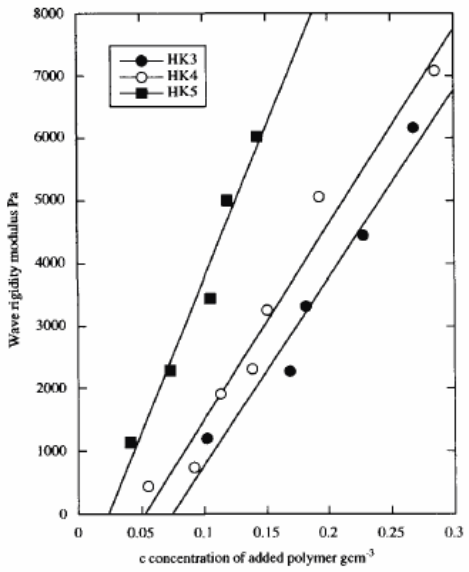

Fig. 20. A plot of the wave rigidity modulus as a function of polymer concentration P28K for four systems: HK3, $\phi = 0.439$; HK4, $\phi = 0.435$; HK5, $\phi = 0.435$.

For the higher molecular weight polymer P8K phase separation does occur at lower polymer concentrations but the form of the separation is complex. This can largely be attributed to particle sedimentation occurring competitively with phase separation particularly with the largest particle sized dispersion HK3. This is an important consideration particularly if similar ratios of $a_{\text{eff}}/R_{\text{g}}$ are compared with particles of different densities. The relative dynamics of the two processes are an important consideration. The data gathered in this study is not comprehensive enough to clarify where these zones occur. They are likely to be concentration dependant. A suggested approach is to define a sedimentation time-scale in terms of the time required for a particle to move a distance a_{eff} when travelling at the Stokes velocity.

$$\tau_{\text{sedi}} = \frac{9\eta(0)}{2\Delta\rho a_{\text{eff}} g} \tag{10}$$

where g is the gravitational acceleration, $\Delta\rho$ the density difference between the particle and the medium. The low shear viscosity has been used to allow for the crowding effects influencing the hydrodynamics. An appropriate time-scale for aggregation τ_{agg} can be defined from the characteristic time to form a doublet using a similar approach to that of Smoluchowski and Fuchs.

$$\tau_{\text{agg}} = \frac{\pi a_{\text{eff}}^3 \eta(0) W}{\phi k T} \tag{11}$$

where W is the stability ratio and depends on the strength of the interaction energy between the particles. In the original derivation it is postulated a repulsive potential barrier exists which prevents touch-stick aggregation of the particles which gives rise to a large value of W. The particles must over come an 'activation energy' barrier in order to aggregate. For an attractive depletion potential acting on quasi-hard spheres the situation is somewhat different. The particles can aggregate but in a secondary minimum. The steric barrier prevents coagulation. In this context W, which is derived from an integral in the pair potential with distance, reflects the ability of particles to escape from the secondary minimum through Brownian collisions. It is consistent with the original approach but will show subtly different features owing to the nature of the aggregation and the potential. The low shear rate viscosity has been incorporated to approximate for concentration and hydrodynamic effects. Thus taking the ratio of these time-scales gives an estimate of the rate of doublet formation versus the time of a single particle sedimenting.

$$S_2 = \frac{2\pi W}{9\phi} \frac{\Delta\rho a_{\text{eff}}^4 g}{kT} \tag{12}$$

If S_2 is much greater than unity the system will sediment before aggregating. For PMMA dispersions at 25°C this expression gives,

$$S_2 = 7.3 \times 10^{21} \frac{W a_{\text{eff}}^4}{\phi}. \tag{13}$$

Now with the addition of free polymer W will reduce from infinity to a value less than unity. There will be a level of polymer addition where W and the volume fraction will take similar values.

This occurs when $a_{eff} = 10^{-6}$ m, i.e. the boundary between aggregation and sedimentation has been reached with respect to doublet formation. If the radius is less than this the system will tend to flocculate rather than sediment.

There are a number of limitations to viewing the system in terms of this dimensionless group. Firstly it only applies to the initial stages of aggregation. So for example consider the aggregation of two doublets. An estimate of the effective radius for a doublet can be obtained by taking the total mass of the doublet and calculating an equivalent radius of a particle of the same material. Using the same assumptions as above the doublet has a greater tendency to sediment and a core particle radius of 400 nm will sediment as a doublet rather than aggregate. This is a similar size to HK3. The radius will continue to drop as the aggregate size increases this being one of the driving forces towards eventual phase separation. Secondly the dimensionless group defined above does not allow for the response of concentrated systems. It does however illustrate the key features and a sensitivity on the interparticle potential through the value of W. The data in Fig. 5 shows a net movement of the sample towards the bottom of the container after 1 month. At concentrations below c^+ the change in sediment after 1 month is consistent with the sedimentation of the PMMA dispersion. At c^+ there is a distinct change in response where depletion has occurred. At high concentrations of polymer sedimentation has been enhanced but not to the same extent. This is presumably due to a complex interplay of factors and in particular the influence of W and concentration.

The data is more readily understood for molecular weights greater than that of P8K. At moderate concentrations of particles phase separation occurs when the polymer addition level exceeds a critical value. A good example of this response is shown in Fig. 3c. This observation was made after 3 days. After 7 months sedimentation dominates the behaviour and two separate phases form. Interestingly the polymer induced phase separation is denoted by a rapid increase in the height of the sedimenting material at c^+. However at greater concentrations the boundary height increases again. This is most likely due to viscous processes preventing the system from acquiring its pseudo-equilibrium structure. This can be rationalised by considering the time to form doublets given in Eq. (12). The time is proportional to the low shear viscosity of the system. For a dilute system of particles this can be replaced by the medium viscosity. However for these systems as the polymer concentration is increased the medium viscosity will increase. Thus τ_{agg} will increase and the rate of phase separation might be expected to reduce. One method of allowing for this change is to multiply the ratio of heights by the ratio of the polymer viscosity to the solvent viscosity. This is effectively reducing the height of the phase boundary to the value it would have achieved had the viscosity of the solvent not been changed by increasing polymer concentration.

$$\frac{H_S}{H_T}(\text{corr}) = \frac{H_S \eta_o}{H_T \eta_p} \qquad (14)$$

In fact this correction would also apply to the additional drag experienced by a particle during sedimentation. An example of the viscous correction applied to Fig. 3(c) is shown in Fig. 21. This clearly illustrates that the corrected sediment boundary is reduced to a constant value for a limited range of polymer concentrations. The viscosity is blocking the attainment of depletion separation. Phase separation curves which display the characteristic shape of Fig. 21 were all successfully reduced to a constant value when the viscous correction was applied. This has important consequences for the observation of the 'restabilisation region' where a transient but long lived phase develops at high polymer concentrations. The tendency for such a phase to be observed depends upon relative sizes, concentrations, the observational time-scale and the polymer dynamics. An example of a metastable phase is shown in Fig. 4 where increasing polymer concentration eventually results in no observable phase separation. The primary objective of the phase separation work was to establish regions where long lived metastable states occur for rheological studies to be performed. The observations made here are consistent with others in the literature [21,30,31] and presumably the poly-

mer viscosity plays a role in the separation of many systems. This is a factor that needs to be explicitly allowed for perhaps using gravitational Peclet numbers.

3.2. Shear stress–shear rate studies

There is a clear distinction in the flow properties between P1K added to the latex and the other polymer systems. For this reason the P1K system will be considered separately from the other systems.

3.2.1. The Bingham yield stress of P1K

The addition of polymer P1K to dispersions of PMMA has resulted in no depletion driven phase separation. The concentrations examined were in excess of any reasonable estimate of c^+. Moreover the addition of polymer to a dispersion reduced the apparent Bingham yield stress, a response not seen with any of the other systems. An explanation for this behaviour can be given if it is recalled that the polymer is added to the dispersions. This is to enable high concentrations of particles to be utilised. For example the data in Fig. 12 was with polymer added to an initial volume fraction of $\phi_{eff} = 0.531$. As has been suggested above the polymer could be treated as if it were an additional solvent diluting the latex. If this were the case then it is possible to predict the apparent Bingham yield stress provided the degree of dilution can be determined. The Bingham equation can be related to the Krieger expression for the viscosity of hard spheres as a function of stress.

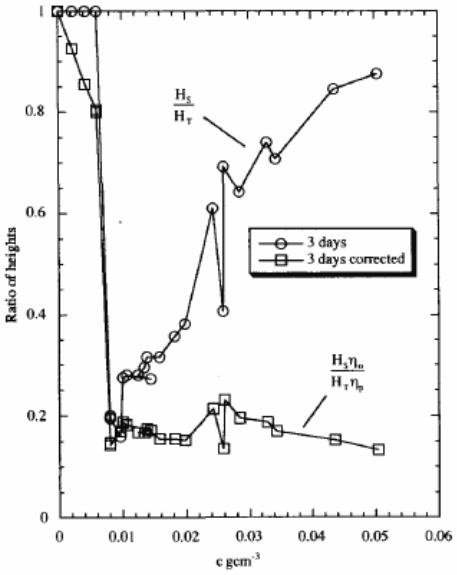

Fig. 21. Phase separation results for HK5 at a volume fraction of $\phi = 0.104$ with the added concentration of the polymer P86K. A viscosity correction has been applied to the data.

$$\eta(\sigma) = \eta(\infty) + \frac{\eta(0) - \eta(\infty)}{1 + b\sigma_r} \tag{15}$$

where b is a constant and σ_r the reduced stress. The value of b = 2.55 can be obtained if it is assumed the Peclet number is unity at that reduced stress where the extrapolated slope of the shear thinning portion of the curve equates to the zero shear viscosity value. The reduced stress is given by:

$$\sigma_r = \frac{\sigma a^3}{kT} \tag{16}$$

Expressing Eq. (15) in terms of stress and equating with the Bingham equation

$$\sigma_B + \eta_{pl}\dot{\gamma} = \eta(\infty)\dot{\gamma} + \frac{\eta(0) - \eta(\infty)}{1 + b\sigma_r}\dot{\gamma} \tag{17}$$

In the high shear limit $\eta_{pl} = \eta(\infty)$ and $b\sigma_r \gg 1$ which gives:

$$\sigma_B = \left(\frac{\eta(0)}{\eta(\infty)} - 1\right)\frac{kT}{ba^3}. \tag{18}$$

So provided the viscosity in the high shear and low shear rates is known the Bingham yield stress can be determined. Using the Krieger–Dougherty expression gives:

$$\frac{\eta(0)}{\eta(\infty)} = \left(\left(1 - \frac{\phi_{eff}}{\phi_m^0}\right)^{-\phi_m^0}\left(1 - \frac{\phi_{eff}}{\phi_m^\infty}\right)^{\phi_m^\infty}\right)^{[\eta]} \tag{19}$$

where $\phi_m^0 = 0.54$ is the low shear packing fraction. Interestingly the Bingham yield stress is independent of the solvent viscosity. The data in Fig. 12 was used to determine the Bingham yield

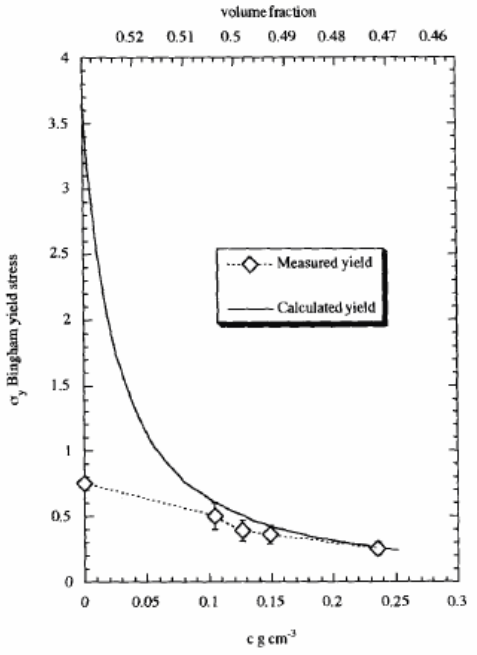

Fig. 22. The Bingham yield stress versus concentration and volume fraction for HK8 at an initial volume fraction of $\phi_{eff} = 0.531$ with the added concentration of the polymer P1K. The experimental data is compared with a model for the Bingham yield stress of hard spheres.

stress. The result of this calculation is shown in Fig. 22. The data is compared with the curves generated using Eq. (18) above allowing for the dilution of the latex by the added P1K polymer. The agreement is good except when no polymer has been added. This disagreement arises from the proximity of the latex concentration to the region of the order disorder transition. In this region the viscosity is very sensitive to the concentration so a small error would readily account for the difference. Another error arises from the extrapolation of the Bingham yield stress which is not totally satisfactory at the highest concentrations and would be better obtained from data gathered over a wider shear rate range. Given these limitations the data strongly supports the notion that P1K is acting not as a depleting polymer but as a diluent.

3.2.2. The Bingham yield stress of P8K to P130K

The Bingham yield stress of these systems all show a linear dependence upon concentration and an intercept at critical concentration c^+. The value of c^+ depends upon the value of ϕ. The statistical mechanical approach of Russel et al. [32] suggests that c^+ is independent of ϕ when the osmotic pressure is relatively low and/or when the ratio of the particle radius to polymer coil radius of gyration is relatively large ($a/R_g \approx 8$–9). Tadros et al. [5] observed rheologically that the dependence of c^+ on ϕ was not well pronounced even for cases where $a/R_g < 8$. In the present case, the smallest possible latex/polymer combination would be latex HK7 with added polymer P115K and this gives $a/R_g = 8$. The $\phi - \sigma_B$ data for a given polymer molecular weight can reduced into a single curve by plotting σ_B/ϕ^2 instead of σ_B. Published data on flocculated systems often display a power law relation between mechanical properties and particle volume fraction although exponential relations have been reported as well. The literature values for the power law index (m) vary between 2.4 and 4.4 for the Bingham yield stress [22]. Tadros et al. [5] have reported an exponent of $m = 2.8$ for sterically stabilised polystyrene latex particles with added poly(acrylic acid). The exponent depends in part on the strength of flocculation and the dynamics of aggregation; lower index values are often indicative of weak flocculation. The low index ($m \approx 2$) obtained in the present work shows that flocculation in the systems is likely to be weak. The different values for the c^+ concentration for different molecular weights means that it is not possible to reduce all data on the same curve. The puzzling feature of the data from the point of view of the pair potential is the presence of an intercept value at c^+. Treatments such as those due to Asakura and Oosawa assume the minimum in the pair potential is a continuous function of osmotic pressure. Assuming there is no asymptotic change in the pressure of the polymer with increasing polymer concentration (and there was none evident in the viscosity) then the attractive energy should also be continuous. So for example considering a simple model as illustrative such as that due to Michaels and Bolger [8] the Bingham yield stress is related to the energy minimum by,

$$\sigma_B \propto \frac{|E_{min}|}{a_{eff}^3}\phi^2 \quad (20)$$

where E_{min} is the depth of the energy minimum. Strictly this was suggested for a strongly aggregated system however it does preserve the notion that as the depth of energy minimum increases the Bingham yield stress should also increase. So at a given volume fraction as the polymer concentration is increased the depth of the energy minimum increases and the Bingham yield stress should increase. The polymer concentration dependence of the Bingham yield stress is linear and thus it is reasonable to suppose that the concentration of E_{min} is linear. In the AO model the value of E_{min} for a system depends directly upon the osmotic pressure of the polymer $\Pi(c)$, at concentration c. Thus for a system with all other variables fixed and only the concentration of polymer changing,

$$\sigma_B \propto \Pi(c) \propto c. \quad (21)$$

In other words the Bingham yield stress depends directly upon the concentration of polymer. It could be argued that a flocculated network does not form until a critical concentration c^+ is reached. This is when the energy well depth is large enough to cause connectivity across the system. If this were the case one would expect the energy of interaction at c^+ to be characteristic of the energy to network, say 10 kT. Using c^+ from the Bingham yield stress data from P8K to P115K the variation in E_{min} from the AO model is from -30 to -45 kT which is a reasonable value to give network formation. However this would also be expected to give substantial flocculation before c^+ at low volume fractions. Therefore phase separation would be observed with these systems below c^+ and so this seems contradictory with the experimental evidence. A self consistent model should demand that at a critical concentration where phase separation occurs the resolved pair potential starts to become substantially attractive. This is not consistent with the AO model for attraction.

3.3. Viscoelastic and shearometry studies

Viscoelastic studies suggest further evidence for a change above c^* or the experimentally defined c^+. It is clear that above c^* there is strong evidence for two relaxation processes. It is tempting to associate these with the diffusion dynamics of the polymer and the particles. These processes are not detected below c^* and so it seems likely that the collective diffusive motion has altered substantially. It is this observation that is key to understanding the apparent pair potential that acts in these systems. Consider increasing the concentration of polymer at a fixed volume fraction of particles. The particles are free to diffuse and will collide. The depletion interaction will ensure they will dwell for a time as a doublet. However the smaller more mobile depleting polymer will also show local and more rapid fluctuations in concentration. Thus the doublet will break apart as the local osmotic pressure due to the polymer falls. This making and breaking will continue until the polymer dynamics begin to slow at about c^*. At this point once aggregation occurs it is no longer energetically favourable for the particle doublet to redisperse. At low particle volume fractions phase separation commences and at high concentration metastable gels form. The time average potential is not substantial until c^* is reached so whilst the AO model would imply doublet formation below c^* this is only as a transient phenomena. An indication of the onset of depletion flocculation might be obtained from a consideration of the diffusional time-scale for the polymer moving through the gap between the particles. The implication is that in order to model macroscopic rheological properties the dynamics of the pair potential must be allowed for in any approach to a depletion potential consistent with say DLVO or steric potentials. This is clearly complex to solve exactly. In the next paper in the series [33] this factor will be accounted for in a new model. There are other difficulties in using the AO model. The shearometry data provides a good approximation to $G(\infty)$ for the network. The high frequency shear modulus is the viscoelastic parameter which is most well found in terms of statistical mechanical modelling. It can be shown that it is proportional to both the first and second derivative of the colloid pair potential [34] for a weakly flocculated network. However the first and second derivatives of the AO poten-

tial are negative giving rise to a calculated aphysical negative modulus for depletion systems. This excludes any relatively small hydrodynamic contributions that might be observed in the frequency range studied. Inclusion of a steric interaction gives rise to a positive moduli but calculations attempted by the authors failed to describe the experimental data for $G(\infty)$ suggesting that the depletion potential itself is again suspect. This issue will be tackled in the next paper.

4. Conclusion

This paper includes a range of experimental data on well characterised systems. A range of molecular weights of polymer have been examined. The diffusion dynamics are important in determining much of the behaviour observed. The polymer P1K acts more like a solvent than a polymer. It did not induce phase separation and reduced the Bingham yield stress on addition to a dispersion. This change is consistent with a reduction in the volume fraction. It is possible this is due to the polymers ability to permeate the grafted layer thus it can never be truly excluded. This clearly has potential consequences for systems of polydisperse polymers where different weight fractions of the polymer act as either a solvent or a depletant. The higher molecular weight systems induced phase separation and metastable phases. The lifetime of the metastable phases is a complex issue but the solvent viscosity is one factor responsible for slowing phase separation. The issue of polymer dynamics is key to the consideration of the observed rheological behaviour. The Asakura–Oosawa potential is not capable of describing $G(\infty)$ or the Bingham yield stress. In the following paper in this series this issue will be addressed more fully.

References

[1] S. Asakura, F. Oosawa, J. Chem. Phys. 22 (1954) 1255.
[2] S. Asakura, F. Oosawa, J. Polymer Sci. 37 (1958) 183.
[3] A. Vrij, Pure Appl. Chem. 48 (1976) 471.
[4] J.F. Joanny, L. Leibler, P.G. de Gennes, J. Poly. Sci. Poly. Phys. Ed. 17 (1979) 1073.
[5] Th.F. Tadros, W. Liang, P.F. Luckham, J. Colloid Interface Sci. 155 (1993) 156.
[6] Th.F. Tadros, W. Liang, P.F. Luckham, J. Colloid Interface Sci. 158 (1993) 152.
[7] Th.F. Tadros, W. Liang, P.F. Luckham, Langmuir 10 (1994) 441.
[8] A.S. Michaels, J.C. Bolger, Ind. Eng. Chem. Fundam. 1 (1962) 153.
[9] C.L. Sieglaff, J. Polymer. Sci. 41 (1959) 319.
[10] P.R. Sperry, H.B. Hopfenberg, N.L. Thomas, J. Colloid Interface Sci. 82 (1981) 6.
[11] L. Antl, J.W. Goodwin, R.D. Hill, R.H. Ottewill, S.M. Owens, S. Papworth, J.A. Waters, Colloids Surf. 17 (1986) 67.
[12] I.M. Krieger, T. Dougherty, J. Trans. Soc. Rheol. 3 (1959) 137.
[13] J.W. Goodwin, R.H. Ottewill, J. Chem. Soc. Faraday Trans. 87 (3) (1991) 357.
[14] D.W. van Krevelen, Properties of Polymers: Their Estimation and Correlation with Chemical Structure, Elsevier Scientific, Amsterdam, 1976.
[15] P.A. Lovell, in: C. Price, C. Booth (Eds.), Comprehensive Polymer Science: Polymer Characterization, vol. 1, Pergamon Press, Oxford, 1989, p. 173.
[16] H.M. Kwaambwa, Ph.D Thesis, University of Bristol, Bristol, UK, 1995.
[17] K.E.J. Barrett (Ed.), Dispersion Polymerization in Organic Media, Wiley, London, 1975.
[18] P.A. Reynolds, C.A. Reid, Langmuir 7 (1991) 89.
[19] P.G. de Gennes, Scaling Concepts in Polymer Physics, Cornell University Press, Ithaca, New York, 1979, p. 255.
[20] M. Doi, S.F. Edwards, Theory of Polymer Dynamics, Claredon Press, Oxford, 1986.
[21] J.W. Goodwin, R.W. Hughes, Adv. Colloid Interface Sci. 42 (1992) 303.
[22] M.J. Van der Aerschot, Colloids Surf. 69 (1992) 15.
[23] W.J. Frith, J. Mewis, T.A. Strivens, J. Colloid Interface Sci. 139 (1990) 55.
[24] D.V. Boger, B. Leary, D.A.R. Jones, J. Colloid Interface Sci. 147 (1991) 479.
[25] D.V. Boger, B. Leary, D.A.R. Jones, J. Colloid Interface Sci. 150 (1992) 84.
[26] B.W. Russel, R.C. Sonntag, J. Colloid Interface Sci. 116 (1987) 485.
[27] M.J. Vold, J. Colloid Sci. 14 (1959) 168.
[28] M.J. Vold, J. Phys. Chem. 64 (1960) 1616.
[29] Y. Tsunashima, M. Hirata, N. Nemoto, M. Kurat, Macromol 21 (1988) 1107.
[30] W.C.K. Poon, A.D. Pirie, P.N. Pusey, Faraday Disc. 101 (1995) 65.
[31] W.B. Russel, M.C. Grant, Phys. Rev. E 47 (1993) 2606.
[32] W.B. Russel, A.P. Gast, C.K. Hall, Faraday Discuss. Chem. Soc. 76 (1983) 189.
[33] Part II this journal next article.
[34] J.W. Goodwin, R.W. Hughes, S.J. Partridge, C.F. Zukoski, J. Chem. Phys. 85 (1986) 559.